Advanced Fiber Materials (2023) 5:1349–1366
https://doi.org/10.1007/s42765-023-00272-w

RESEARCH ARTICLE

N-Cadherin-Functionalized Nanofiber Hydrogel Facilitates Spinal Cord Injury Repair by Building a Favorable Niche for Neural Stem Cells

Kaiyuan Yang[1,2] · Jia Yang[1] · Weitao Man[2] · Zhe Meng[2] · Chun-Yi Yang[1] · Zheng Cao[1] · Jun Liu[1] · Kunkoo Kim[1] · Yaosai Liu[2] · Shuhui Yang[3] · Yi Guo[2] · Zhijun He[2] · Chao Ma[2] · Guihuai Wang[2] · Xiumei Wang[1]

Received: 3 November 2022 / Accepted: 12 February 2023 / Published online: 13 March 2023

Abstract

The inhospitable niche at the injury site after spinal cord injury (SCI) brings several challenges to neural stem cell (NSC) therapy, such as limited NSC retention and neuronal differentiation. Biomaterial-based stem cell transplantation has become a promising strategy for building a favorable niche to stem cells. Herein, an aligned fibrin nanofiber hydrogel modified with N-Cadherin-Fc (AFGN) was fabricated by electrospinning and biochemical conjugation to deliver NSCs for SCI repair. The AFGN hydrogel provides multimodal cues, including oriented nanofibrous topography, soft stiffness, and specific cell binding ligand, for directing NSC functions and nerve regeneration. The conjugated N-Cadherin-Fc recapitulated the homophilic cell–cell interaction for NSCs' adhesion on AFGN and modulated cellular mechanosensing in response to AFGN for NSC differentiation. In addition, the AFGN hydrogel carrying exogenous NSCs was implanted in a rat 2 mm-long complete transected SCI model and significantly promoted the grafted NSCs retention, immunomodulation, neuronal differentiation, and in vivo integration with inherent neurons, thus finally achieved renascent neural relay formation and an encouraging locomotor functional recovery. Altogether, this study represents a valuable strategy for boosting NSC-based therapy in SCI regeneration by engineering an NSC-specific niche.

Keywords N-cadherin · Aligned fibrin nanofiber scaffold · Niche · Neural stem cell · Spinal cord injury

Introduction

Spinal cord injury (SCI) is a devastating case leading to irreversible deficits in motor and sensory functions, posing a worldwide threat to individuals and public health [1]. During the last decade, neural stem cell (NSC)-based tissue engineering therapies have been widely recognized as a promising tactic for nerve regeneration and lost function reconstruction after SCI [2]. Following transplantation into injury sites, exogenous NSCs can differentiate into neural cells and replenish the disastrous loss of neural cells after SCI [3]. Moreover, NSCs can act as a nanomaterial factory that continuously provides various neurotrophic factors and exosomes, which encourages axon re-extension and synapse reformation [2]. However, due to the inhospitable niche at the injury site after SCI, the low-grafted NSC retention and neuronal differentiation extremely restrict the efficiency of NSC transplantation therapy [4]. Hence, reconstructing a desirable niche for NSCs has attracted much attention in NSC-based SCI therapies [5–7].

Kaiyuan Yang, Jia Yang, and Weitao Man have contributed equally to the work.

✉ Guihuai Wang
guihuai_wang@163.com

✉ Xiumei Wang
wxm@mail.tsinghua.edu.cn

[1] State Key Laboratory of New Ceramics and Fine Processing, Key Laboratory of Advanced Materials, School of Materials Science and Engineering, Tsinghua University, Beijing 100084, China

[2] Department of Neurosurgery, Beijing Tsinghua Changgung Hospital, School of Clinical Medicine, Tsinghua University, Beijing 102218, China

[3] School of Materials Science and Engineering, Zhejiang-Mauritius Joint Research Center for Biomaterials and Tissue Engineering, Zhejiang Sci-Tech University, Hangzhou 310018, China

Recently, biomaterial scaffolds have not only served as a platform to bridge the nerve gap after SCI but also been actively used to engineer stem cell niche characteristics [8, 9]. Biologically compatible materials, such as fibrin, collagen, polypeptides, and chitosan, could simulate the extracellular matrix (ECM), providing biophysical and biochemical cues to guide nerve regeneration [10–13], and have been widely investigated for regulating stem cell behaviors and differentiation fate [14, 15]. For example, many studies have indicated that scaffolds with aligned nanoscale topography mimicking the highly oriented structure of nerve fibers could better promote axon sprouting and affect cell fates [16]. Moreover, an increasing number of studies have shown that the combination of different types of cues delivered by biomaterial scaffolds is more promising in cell delivery and tissue regeneration than the single cue release strategy [6, 11]. Thus, in this study, we aimed to develop a novel biofunctional scaffold that represents multimodal cues to better reconstruct the NSC niche and guide axon regeneration.

As a significant component of the ECM, fibrin offers excellent biocompatibility, tunable degradability, suitable flexibility, and plasticity [17, 18]. Moreover, fibrin contains many binding sites for ECM proteins as well as growth factors and cell receptors, making fibrin a promising modifiable cell–carrier matrix and candidate for tissue engineering [19]. Over the past 10 years, various fibrin scaffolds have demonstrated strong potential for SCI repair [3, 18, 20]. For example, a recent study reported that collagen-fibrin hydrogel exhibits better mechanical properties and adhesive strength than single collagen hydrogel, and this composite hydrogel accelerated endogenous NSC migration and SCI repair [21]. In our previous study, an aligned fibrin nanofiber hydrogel (AFG) was constructed by electrospinning, which generated a nanoscale linearly ordered structure and soft elasticity mimicking native nerve ECM. Furthermore, the 3D nanoscale construction of AFG provides a high surface area for cell attachment and growth [22]. We found that AFG could promote the neurogenic differentiation of mesenchymal stem cells (MSCs) and activate the oriented neurite project of rat dorsal root ganglion (DRG) neurons rapidly in vitro [22]. In animal experiments, AFG was also proven to facilitate axon regeneration and motor functional recovery in rodent and canine SCI models [23, 24]. However, AFG lacks specific biochemical cues to re-engineer the NSC desirable niche, which could coax the grafted NSCs' retention and neuronal differentiation.

Biochemical cues, such as soluble neurotrophic factors and cell adhesion molecules (CAMs), play critical roles in constructing stem cell niches, regulating stem cell fate, and accelerating axon regeneration and are widely applied in biomaterial functional modification as well as bioactive interface creation [15]. In recent years, studies on cadherins, an important family of CAMs, have made tremendous advances in tissue engineering [25]. N-Cadherin (NCAD), a type of cadherin that exists in the central nervous system (CNS), plays a crucial role in proper CNS development, neurite sprouting, and axon regeneration [26]. NCAD is a homophilic transmembrane glycoprotein that mediates cell–cell adhesive contacts and modulates the cell–matrix mechanical response, which has been accepted as a vital determinant of stem cell fate [27–29]. The cytoplasmic regions of NCAD can form a cadherin–catenin complex by binding to α-catenin and β-catenin [30]. The complex anchors actin filaments (F-actin) that allow the cytoskeleton to sense and respond to mechanical coupling across the cell membrane modulate cell adhesion and migration [30, 31]. In addition, NCAD also encourages axon outgrowth and dendritic arborization through fibroblast growth factor receptor (FGFR) activation [27, 32]. Notably, during the development of the CNS, NCAD expressed on the surface of NSCs regulates NSC adhesion and differentiation [33]. Moreover, NCAD-maintained adhesion could promote the differentiation of NSCs toward neurons by regulating the Wnt/β-catenin and AKT signaling pathways [34, 35]. To better utilize and present NCAD in tissue engineering, recombinant N-cadherin human Fc chimeric protein (NCAD-Fc) was constructed [36]. NCAD-Fc contains the extracellular domain of NCAD and the Fc domain of human immunoglobulin (IgG). The Fc domain could enhance the activity, stability, and solubility of NCAD [37]. Furthermore, the Fc domain enables NCAD to immobilize onto substrates via hydrophobic interactions, protein A (PA) affinity capture, or antigen–antibody interactions [36, 38, 39]. Therefore, the NCAD-Fc-conjugated bioactive scaffold may be an attractive platform for NSC delivery, where NSCs can be retained in a desirable niche and differentiate toward neurons. Nevertheless, current studies mainly focused on NCAD-Fc as a cofactor for maintaining cell adhesion cultures or promoting NSC neuronal differentiation on two-dimensional interfaces in vitro [26, 31, 36, 40], and the potential of NCAD-Fc-conjugated bioactive scaffolds modulating the grafted NSC niche as a combinatorial strategy to promote SCI repair is overlooked.

In the present study, we modified AFG with NCAD-Fc via biochemical conjugation to successfully obtain a novel multifunctional scaffold AFG-NCAD-Fc (AFGN) to carry exogenous NSCs for spinal cord regeneration [10, 38, 41]. The AFGN hydrogel exerts synergistic multimodal biophysical and biochemical cues, including linearly ordered nanoscale topography, soft stiffness, and NCAD presented biological activity, which worked together and eventually rebuilt the favorable niche for the NSCs. Subsequently, NSC adhesion and neuronal differentiation on the AFGN hydrogel were evaluated in vitro. Furthermore, the AFGN hydrogel carrying exogenous NSCs was implanted into a rat 2 mm-long complete transected SCI model to bridge the stumps. Structural reconstruction, axon regeneration,

neurogenesis, and functional recovery were investigated based on morphological, histological, electrophysiological, and locomotor parameters.

Experimental Section

Fabrication of AFGN Hydrogel

AFG was generated by electrospinning as previously described [10]. In brief, 2% (w/v) fibrinogen (F8630, Sigma-Aldrich, USA) with 0.5% (w/v) poly(ethyleneoxide) (PEO, 4000 kDa, Sigma-Aldrich, USA) in distilled water was electrospun and collected in a liquid bath with 50 mM $CaCl_2$ and 5 units/mL thrombin (T4648, Sigma-Aldrich, USA) according to the following conditions: 23 G needle, a voltage of 4 kV, rotating collector at a speed of 60 rpm. Subsequently, the AFG fibers were assembled to form a 2 mm-thick bundle for further uses. After removal of PEO from the AFG by washing with distilled water, the AFG was exposed to ultraviolet light overnight for sterilization. The immobilization method was modified from protocols published previously and performed under sterile conditions [38, 41, 42]. The COOH groups of the AFG were activated and stabilized in a solution of 0.4 mg/mL 1-ethyl-3-(dimethylaminopropyl) carbodiimide hydrochloride (EDC) (Sigma-Aldrich, USA)/0.6 mg/mL N-hydroxysuccinimide (NHS) (Sigma-Aldrich, USA) for 30 min at room temperature. The AFG was then rinsed three times with distilled water for 15 min. Afterward, the AFG was coated with 2 μg/mL protein A (PA) (21,181, Pierce, USA) solution for 2 h at 37 ℃. Following three washes, the AFG was finally soaked in 10 μg/mL recombinant human N-cadherin human Fc chimera protein (NCAD-Fc, SOMAR, Japan) solution for 12 h at 37 ℃, forming a novel functional hydrogel named AFG-NCAD-Fc (AFGN). All procedures were performed under sterile conditions.

Characterizations of AFGN Hydrogel

Proton nuclear magnetic resonance (^{1}H NMR) was applied to verify the conjugation of AFG and AFGN. The AFG and AFGN powders were dissolved in deuterium oxide (D_2O) at a concentration of 10 mg/mL. The ^{1}H NMR spectra were recorded on a 600 M NMR spectrometer (JNM-ECA600, JEOL Ltd., Japan) at room temperature. For Fourier transform infrared (FTIR) spectrometry, the freeze-dried AFG and AFGN hydrogels were ground into fine powders. The FTIR spectra were recorded from 4000 to 400 cm^{-1} on an FTIR spectrometer (X70, NETZSCH, Germany) using KBr pellets. To observe the microstructure of the AFG and AFGN hydrogels, the hydrogels were fixed in cold 2.5% (v/v) glutaraldehyde for 3 h and dehydrated by an ethanol series. After lyophilization for 24 h, the samples were characterized by scanning electron microscopy (SEM, Carl Zeiss, GEMINISEM 500, Germany). The binding rate of NCAD-Fc immobilized onto the AFGN was determined using a human N-cadherin ELISA Kit (MM-13240H2, MEIMIAN, China) by subtracting the concentration of uncombined NCAD-Fc from the initial concentration, as previously described [43].

The rheological properties of the AFG and AFGN were examined using an 8 mm-diameter parallel plate at 37 ℃ (Physical MCR301 rheometer, Anton Paar GmbH, Graz, Austria). The dynamic frequency sweep test (0.1–10 Hz at 1% strain) was used to record the storage (G′) and loss (G″) modulus. The stiffness of the AFG and AFGN hydrogels was assessed by atomic force microscopy (AFM, Dimension ICON, Bruker, Billerica, MA, USA). Force curves from 500 randomly chosen points per hydrogel were registered using silicon SNL-D probes consisting of 20 μm-diameter glass beads attached to the edge of a silicon nitride V-shaped cantilever with a nominal spring constant of 0.06 N/m. The Young's moduli of the hydrogel surfaces were evaluated from the force-indentation curves by fitting to the Hertz model. The water contact angle of the AFG and AFGN was measured using an OCAH200 Optical contact angle tester (Dataphysics, German), as previously described [44].

In Vitro NSC Isolation and Culture Experiment

NSCs were isolated from fetal (embryonic Day 14) SD rats under sterile conditions, as previously described with slight modifications [45]. In brief, the hippocampus of the embryo was dissected on ice gently to strip the endocranium and blood vessels. After dissection, the hippocampal tissues were transferred to a dish with ice-cold PBS and cut into small pieces, digested in 0.05% EDTA/Trypsin (Gibco, USA) at 37 ℃ for 10 min, and centrifuged at 200×*g* for 5 min. The cell suspension was cultured in neurobasal medium (Gibco, USA) containing 2% B27 (Gibco, USA), 1% penicillin–streptomycin (PS, Sigma-Aldrich, USA), 20 ng/mL epidermal growth factor (EGF, Solarbio, China), and 20 ng/mL basic fibroblast growth factor (bFGF, Solarbio, China). Afterward, NSCs were kept in an incubator containing 5% CO_2 at 37 °C, and half of the medium was changed every 2 days. Seven days later, the newly formed NSC spheres were digested into single cells with Accutase (Invitrogen, USA). Single NSCs were cultured using DMEM/F12 proliferative medium-containing 2% B27 (Gibco, USA), 1% N2 (Gibco, USA), 1% PS (Sigma-Aldrich, USA), 20 ng/mL EGF (Solarbio, China), and 20 ng/mL bFGF (Solarbio, China). Cultured NSCs were collected for in vitro NSC adhesion and

differentiation experiments. For in vivo transplantation, the NSCs were incubated with DMEM/F12 proliferative medium-containing lentiviral particles (pLV-EGFP/Puro-CMV, Cyagen Biosciences, China) and polybrene (5 μg/mL) at a multiplicity of infection (MOI) of 50 for 16 h to obtain GFP-labeled NSCs. In addition, some NSC spheres at 7 days were randomly collected and stained with Nestin (1:100, sc-23927, Santa Cruz, USA) for the identification of NSCs, and images were taken with confocal laser scanning microscopy (LSM980 Airyscan2, Zeiss, Germany).

Seeding of NSCs onto the Hydrogels In Vitro

To identify NSC adhesion, single NSCs were resuspended in DMEM/F12 culture medium-containing 1% PS (Sigma-Aldrich, USA) and 10% fetal bovine serum (FBS, Gibco, Australia) to promote NSC adhesion, and then seeded onto the AFG and AFGN hydrogels at a density of 1×10^5 cells per scaffold and cultured in an incubator containing 5% CO_2 at 37 °C. After culturing for 1 day, 3 days, and 7 days, the samples were gently washed with PBS and then fixed in 4% paraformaldehyde (PFA) for 1 h at 4 °C. Subsequently, the NSCs retained on the hydrogels were permeabilized with 0.1% Triton X-100 for 20 min and blocked with 10% normal goat serum (Solarbio, China) for 1 h. Then, the samples were incubated with rhodamine phalloidin (RP, Solarbio, China) and DAPI (sc-74421, Santa Cruz, USA) for 40 min. Images were captured by confocal laser scanning microscopy (LSM980 Airyscan2, Zeiss, Germany). Meanwhile, the NCAD-Fc release during the cell culture process was assessed. The culture medium of NSCs on the AFGN was collected and refreshed every day. An ELISA kit was used to quantify the released concentration of NCAD-Fc.

To identify NSC differentiation, single NSCs were resuspended in the DMEM/F12 culture medium-containing 1% PS and 10% FBS to promote NSC differentiation and then seeded onto the AFG and AFGN hydrogels at a density of 1×10^5 cells per scaffold. Moreover, the NSCs seeded on the TCP in the culture medium with or without 50 ng/mL nerve growth factor (Solarbio, China) as for positive control (PC) or negative control (NC) group, respectively. After 7 days of culture at 37 °C, the samples were washed with PBS, fixed in 4% PFA, permeabilized by 0.1% Triton X-100, and blocked with 10% normal goat serum sequentially. Then, the samples were immunostained with Tuj-1 (1:500, ab18207, Abcam, UK) and GFAP (1:500, ab4648, Abcam, UK) primary antibodies for 16 h at 4 °C, followed by incubation with corresponding secondary antibodies and DAPI at room temperature for 40 min. Images were taken with a confocal laser scanning microscope (LSM980 Airyscan2, Zeiss, Germany).

Furthermore, after 7 days of culture, the total RNA of NSCs from the NC, PC, AFG, and AFGN group was isolated by an mRNA kit (Tiangen, China), and then reversed to cDNA using a FastQuant RT kit (Tiangen, China), for a quantitative real-time polymerase chain reaction (qRT-PCR). The qRT-PCR was performed using SYBR Green supermix (Bio-Rad, USA) and detected by the CFX96 real-time PCR detection system (Bio-Rad, USA). The relative gene expression was normalized by the GAPDH and determined by the $2^{-\Delta\Delta Ct}$ method [46]. The primer sequences are listed in Table S1.

The Immunoregulation Experiment in Vitro

The rat HAPI microglia cells (a generous gift from Professor Li-Na Zhang, Department of Critical Care Medicine, Xiangya Hospital, Central South University, China) were cultured in Dulbecco's Modified Eagle's Medium (high glucose, DMEM, Pricella) which contained 10% FBS and 1% PS, in an incubator containing 5% CO_2 at 37 °C. The HAPI cells were seeded on the TCP control (TCP group) and AFGN hydrogel (AFGN group) at a density of $1 \times 10^5/cm^2$. Meanwhile, the HAPI and NSC cells (5×10^4 cells/insert) were separately seeded into a 24-well transwell system (Corning, 0.4 μm pores, USA) (NSC group). Followed by adhesion for 12 h, the HAPI cells were stimulated by adding 1 μg /mL lipopolysaccharide (LPS, Invivogen, France) and 20 ng/mL interferon-γ (IFN-γ, adcam, UK) in a DMEM-F12 medium for 24 h to polarize. Subsequently, the total RNA was extracted from the HAPI cells of all groups, respectively, and analyzed by the qRT-PCR assay. The primer sequences are listed in Table S1.

Animal Procedures

Animal experiments were performed in accordance with the Guide for the Care and Use of Laboratory Animals formulated by the National Institutes of Health (NIH) and were approved by the Institutional Animal Care and Use Committee of Tsinghua University (Beijing, China). Healthy female SD rats (8 weeks old, 200–230 g, $n = 104$) were used in this study. Surgeries were performed under anesthesia with an intraperitoneal injection of 1% w/v pentobarbital sodium solution (30 mg/kg) to establish the rat SCI model. Briefly, a dorsal laminectomy was performed to remove the T8–T10 vertebrae. Under a microscope, a 2 mm-long block of the T9 spinal cord was completely transected and removed using microscissors. The ventral dura mater was preserved, and gel foam was used for hemostasis. All animals were randomly divided into four groups according to different treatments. AFGN hydrogel (AFGN group), 10 μL of cell suspension containing 1×10^6 GFP-labeled NSCs (NSC group), 10 μL of saline (control group), or AFGN hydrogel with 1×10^6 GFP-labeled NSCs (AFGN-NSC group) was immediately implanted into the lesion site to fill the gap.

Finally, the surgical incisions were closed with sutures. After the operation, all animals received meloxicam (4 mg/kg) for 3 days and penicillin for 7 days. Manual bladder extrusion was applied three times a day until automatic micturition recovered.

Histological Evaluation

At 1 week, 4 weeks, 8 weeks, and 12 weeks postsurgery, rats were sacrificed and consecutively perfused with saline and 4% w/v PFA after pentobarbital anesthesia, and the spinal cord tissue segments containing the lesion epicenter were collected. Moreover, bladder, heart, liver, spleen, lung, and kidney tissues were also harvested. Tissue samples were fixed in 4% w/v PFA at 4 °C overnight and successively placed into sucrose solution (30% sucrose in 0.1 M PBS) at 4 °C for 72 h. Tissue samples were separately embedded in OCT compound and sliced into 10 μm-thick histologic sections using a cryostat microtome (CM 1950, Leica, Germany). These tissue sections were used for hematoxylin and eosin (H&E) staining, Masson staining, and immunofluorescence staining. Images of H&E or Masson staining were taken with a Pannoramic SCAN scanner (3DHIESTECH, Hungary) and processed using CaseCenter 2.9SP1 software (3DHIESTECH, Hungary). For immunofluorescence staining, the sections were rinsed with PBS and then immersed in PBS containing 10% w/v normal goat serum and 0.3% w/v Triton X-100 for 2 h at room temperature. Then, the sections were incubated with primary antibodies (Table S2) at 4 °C overnight, washed with PBS, and incubated with the corresponding secondary antibodies (Table S1) for 1 h in the dark. DAPI (Abcam, UK) mounting medium was used to stain cell nuclei. Images of immunofluorescence staining were collected on a Zeiss Axio Scan Z1 scanner (Carl Zeiss, Germany) and processed using Zen 2.6 (Blue edition) software (Carl Zeiss, Germany) under the same parameters. ImageJ 1.51 k (Wayne Rasband, NIH, USA) was used for quantitative analysis of the representative immunofluorescence and H&E images.

At 12 weeks postoperatively, the lesion epicenters in the other 12 rats (3 rats for each group) were retrieved and sliced into 60 nm-thick ultrathin axial sections or 500 nm-thick semithin axial sections using a microtome (EM UC6, Leica, Germany) for further detection of myelination, axon regeneration, and synapse ultrastructure [24, 47]. The semithin sections were stained with toluidine blue/borax solution and scanned using a Pannoramic SCAN scanner (3DHIESTECH, Hungary). The ultrathin sections were doubly stained with lead citrate and uranyl acetate, and images were captured by a transmission electron microscope (TEM, Tecnai Spirit, FEI, Czech Republic). ImageJ 1.51 k (Wayne Rasband, NIH, USA) was used for quantitative analysis of the representative toluidine blue staining and TEM images.

Functional Behavior Analysis

During the 12 week repair period, locomotor function was evaluated weekly by two independent observers blinded to the conditions using the Basso–Beattie–Bresnahan (BBB) rating scale [48]. The rats ($n = 8$ for each group at each time point) were placed into an open field (100 cm diameter) and observed for 5 min. The hindlimb movements of each rat were scored and recorded. Moreover, the gait was recorded at 12 weeks postsurgery using Catwalk XT 10.6 System (Noldus, Wageningen, The Netherlands) [24]. CatWalk 10.6 software labeled paw prints automatically for further analysis.

Electrophysiological Evaluation

Motor-evoked potentials (MEPs) were carried out using Electromyograph and Evoked Potential Equipment (33A07, Dantec Dynamics, Denmark). All rats received the same anesthesia procedure during surgery and electrophysiological evaluation. The transcutaneous bipolar needle electrodes were positioned on the skull surface to induce MEPs. The recording needle electrodes were placed into the tibialis anterior muscle, and then, the grounding electrode was placed into the back subcutaneously. The peak amplitude and latency of the MEPs were measured and compared among the groups.

Statistical Analysis

Statistical analysis was carried out in SPSS Statistics for Windows (v.23.0; IBM Corp., USA). All data are presented as the mean ± standard deviation (SD) unless otherwise indicated. One-way analysis of variance (ANOVA) followed by LSD (equal variances) or Dunnett's T3 post hoc test (unequal variances) was performed to determine significant differences for multiple comparisons. Two-way repeated-measures ANOVA was used to compare significant differences between each group and time point in the BBB experiment. All tests were two-sided, and a P value < 0.05 indicated a statistically significant difference.

Results and Discussion

Fabrication of AFGN Hydrogel

AFG was generated by electrospinning as described in our previous studies [10]. Afterward, NCAD-Fc was immobilized onto AFG via biochemical conjugation, forming the functionalized AFGN hydrogel (Fig. 1a and S1a). Compared with chemical crosslinking, biochemical conjugation

with PA is more advantageous in preserving the function of NCAD-Fc [25]. The successful conjugation of NCAD-Fc to the AFG was examined by ^{1}H NMR (Fig. 1b) and FTIR spectrometry (Fig. 1c). The ^{1}H NMR spectra of AFGN showed extra peaks at 2.5 ppm corresponding to the introduction of a characteristic methylene group by NCAD-Fc, which was absent in AFG. In addition, the FTIR spectra showed characteristic peaks at 1639 cm^{-1} in the AFGN, reflecting the preserved β-sheet structure due to biochemical conjugation. SEM images showed nanoscale aligned fibrous structures in both AFG and AFGN hydrogels (Fig. 1d and S1b), exerting biophysical cues by mimicking the linearly ordered ECM in the spinal cord. The rheological measurement results indicated that the AFG and AFGN hydrogels remained steady under constant deformation and exhibited similar viscoelasticity properties (Fig. 1e, f), which were close to the viscoelasticity of soft tissue (tanδ~10–20%) [49]. The Young's moduli of the AFG and AFGN hydrogels were 1.22 ± 0.17 kPa and 1.18 ± 0.06 kPa (Fig. 1g), respectively, which were similar to the moduli of the ECM in native nerve tissue (~1–4 kPa) [50–52]. The ELISA results demonstrated that the binding rate of NCAD-Fc immobilized onto the AFGN hydrogels was 28.1 ± 4.6% (Fig. S1c). The water contact angles of the AFG and AFGN were $65.90 \pm 4.70°$ and $50.87 \pm 8.08°$, respectively (Fig. S1d). These results demonstrated that the NCAD-Fc was successfully immobilized onto the AFGN hydrogels and enhanced the hydrophilicity of the hydrogel.

In Vitro Modulation of NSC Adhesion and Differentiation by the AFGN Hydrogel

NSCs were isolated from the hippocampus of embryonic SD rats [45]. After culturing for 7 days, the newly formed NSCs neurospheres (Fig. S2a) were identified by Nestin (NSC marker). As expected, the cells in neurospheres were almost totally Nestin-positive (Fig. S2b), confirming their NSC nature. To investigate NSC adhesion on different hydrogels, NSC neurospheres were digested into single cells and seeded onto the AFG and AFGN hydrogels. Interestingly, we observed obvious differences in cell morphology on the AFG and AFGN. Starting from day 1 after cell seeding, the cytoskeletons of cells cultured on the AFGNs began to elongate along fibrin nanofibers, while those on the AFGs still showed inconspicuous prior orientation. Over time, we observed that AFGN remarkably enriched more cells than AFG, and cells on the AFGN presented increasingly directed elongation on day 3. After 7 days of cell culture, abundant cells overlying the surface of AFGN exhibited impressive time-evolving elongated morphology and well-developed cytoskeleton actin filaments that highly coaligned with the long axial direction of AFGN nanofibers (Fig. 1h). Based on previous research, the extracellular domains of N-cadherin could bind to each other through homophilic interaction to construct the structure of focal adhesion (FA) and adherens junction (AJ), which are necessary conditions to mediate cell–ECM interaction and cell–cell adhesion [29, 33]. Meanwhile, the intracellular regions of NCAD could interact with p120 catenin and indirectly bind to the actin filaments (F-actin), which enables cells to sense and feedback to the biophysical cues of the substrate and modulates cellular matrix mechanosensing through the FAK/AKT/YAP pathway [25, 33]. Therefore, we conducted qRT-PCR to evaluate the relevant gene expression in NSCs after culturing 7 days on different hydrogels. As shown in Fig. S3, the gene expression of the adhesion specific markers (YAP, p120, AKT, and Actin) exhibited greater up-regulation in AFGN group in comparison to AFG group. Our findings are in agreement with the previous studies, indicating that AFGN could significantly promote cell adhesion, modulate cellular matrix mechanosensing, and adjust the actin cytoskeleton in response to the aligned nanoscale topographies of the fiber matrix and promote the cell directional elongation.

Furthermore, we examined the differentiation potential of NSCs in the NC, PC, AFG, and AFGN groups using Tuj-1 (β-tubulin III, early neuron marker) and glial fibrillary acidic protein (GFAP, astrocyte marker) antibodies after 7 days of culture. As shown in Fig. S4a, compared with the NC group, cells of PC group exhibited significantly increased positively stained for Tuj-1 with the induction of nerve growth factor. However, cells of both NC and PC groups were oriented in random directions. In contrast, cells on the AFG showed positive staining for both Tuj-1 and GFAP with a certain degree of elongation along the direction of the fibers, whereas cells on the AFGN exhibited increased, obviously elongated and oriented Tuj-1-positive staining with relatively weak GFAP expression. Meanwhile, qRT-PCR were conducted to evaluate the relevant gene expression in NSCs after culturing on the different substrates (Fig. S4b). It was shown that in the AFGN group, the gene expressions of the neuronal lineage markers (Tuj-1, NSE, and NeuN) were significantly increased when compared with other groups, but the MAP-2 (mature neuron marker) gene expression showed no statistical difference between the AFG and AFGN group. Moreover, compared with the NC and AFG group, the GFAP gene expression decreased obviously in the AFGN group. These results indicated that AFGN could promote the neuronal differentiation of NSCs in vitro through the enhanced cell–ECM interaction and cell–cell adhesion as well as adhesion-mediated mechanical feedback [29].

In addition, the release of NCAD-Fc from AFGN during the cell culture was also investigated by ELISA. As shown in Fig. S5, comparing with the initial binding concentrations of NCAD-Fc detected, more than 97% NCAD-Fc was

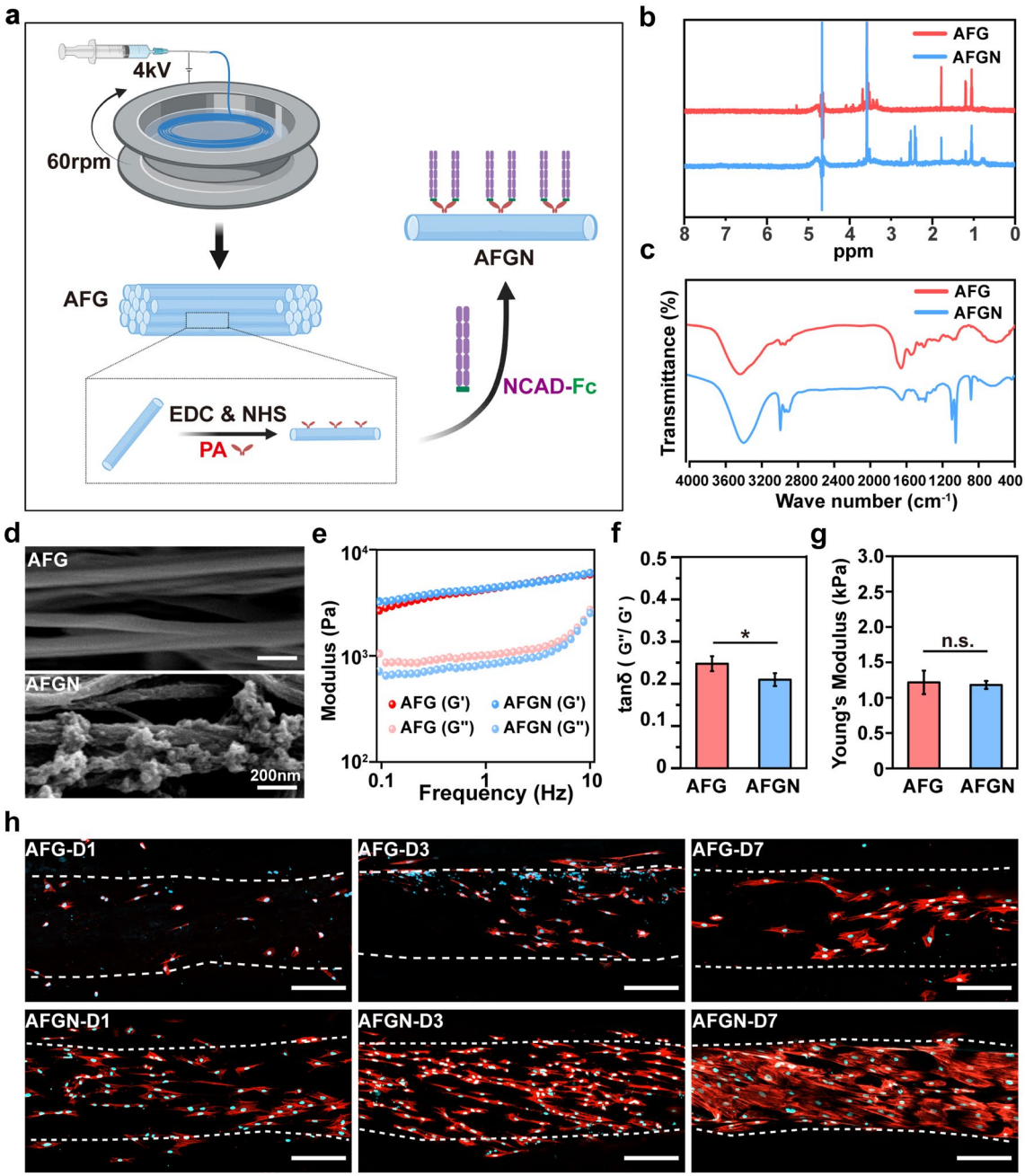

Fig. 1 The fabrication and characterization of the AFGN hydrogel. **a** Schematic diagram of the fabrication of AFGN hydrogel, **b** ^{1}H NMR spectra of AFG and AFGN, **c** representative FTIR spectra of AFG and AFGN hydrogels, **d** SEM images of AFG and AFGN hydrogels, **e** rheological measurements of storage (G′) and loss (G″) modulus of AFG and AFGN, **f** tanδ (G″/G′) at 1 Hz of AFG and AFGN, **g** Young's moduli of AFG and AFGN hydrogels measured by atomic force microscopy (AFM). $^{*}P<0.05$; n.s. no significant; $n=3$, and **h** representative cytoskeleton F-actin (stained with rhodamine phalloidin, red) staining images of NSCs on AFG and AFGN cultured for 1 day, 3 days, and 7 days, respectively. The nuclei were stained with DAPI (blue). Scale bar represents 100 μm

remained on the AFGN after culturing for 7 days, indicating that the NCAD-Fc can be stably immobilized on the AFGN hydrogels.

In Vivo Implantation and Motor Functional Recovery Evaluations

The effects of the AFGN hydrogel on spinal cord regeneration and NSC desirable niche reconstruction were evaluated through implantation in a rat 2 mm T9 complete transection

SCI model (Fig. S6). After SCI, the rats were kept for 12 weeks (Fig. 2a) and divided into four groups as follows: rats that received AFGN hydrogel implantation (AFGN group), rats that received GFP-labeled NSC implantation (NSC group), those that received GFP-labeled NSCs carried by AFGN hydrogel (AFGN-NSC group), and the control group (merely received saline) (Fig. 2b). To evaluate the locomotor function recovery of hindlimbs, the BBB rating test was performed weekly after surgery, and the paw prints of the rats at 12 weeks postsurgery were recorded using CatWalk XT 10.6 System. From 2 weeks postsurgery, the mean BBB score of the AFGN-NSC and AFGN groups exhibited a significant improvement, especially the AFGN-NSC group, to almost 9 at 12 weeks postsurgery (Fig. 2c). However, the BBB scores of the NSC and control groups displayed no obvious increase during the 12 weeks. In particular, at 12 weeks postsurgery, rats in the AFGN-NSC group could make occasional weight-supported plantar steps (Fig. 2d, e) and forelimb–hindlimb coordination (Fig. 2e), whereas in the NSC and control groups, the rats displayed persistent dragging of the hindlimbs without weight support.

Motor function recovery was further confirmed by performing electrophysiological analyses. The cortical MEPs exhibited approximately 2.1 mV amplitude and 3.0 ms latency before SCI and disappeared completely after surgery, indicating that the rat SCI model was successfully established. Although none of the four groups recovered to normal levels at 12 weeks after surgery, a significantly shorter latency and higher amplitude were detected in the AFGN-NSC group than in the other groups (Fig. 2f, g),

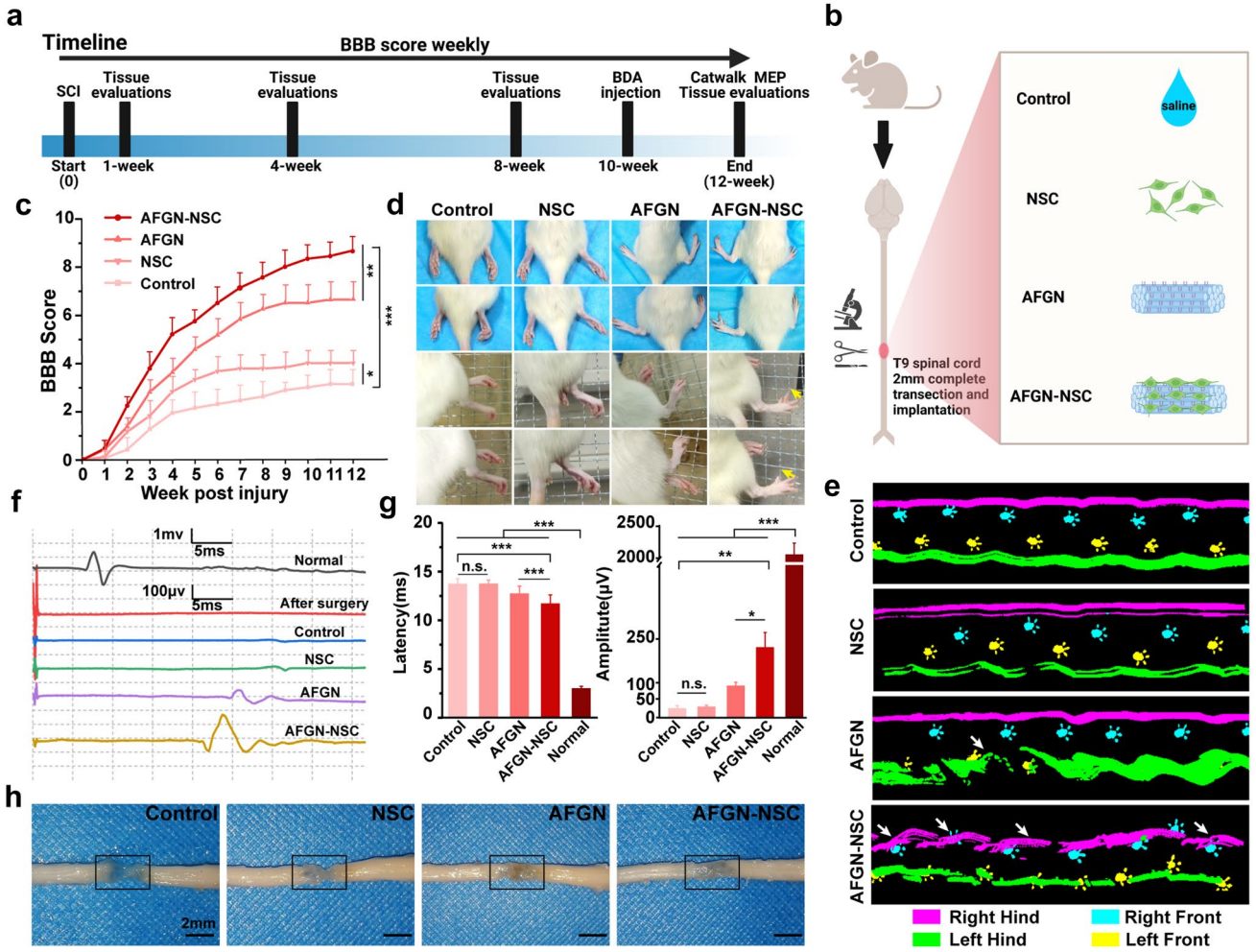

Fig. 2 Functional and electrophysiological recovery evaluations in vivo. **a** Timeline of the experiments in vivo, **b** schematic of different graft-based grouping of the experiments in vivo, **c** the BBB scores of rats in each group, $^{*}P<0.05$, $^{**}P<0.01$, $^{***}P<0.001$; n = 8, **d**, **e** typical records of rat walking gaits (**d**) and the Catwalk footprint depiction (**e**) 12 weeks postsurgery, **f** representative MEPs traces of normal rats, rats immediately after surgery and of each group, and **g** quantitative analysis of MEPs latency and amplitude. Data are presented as the mean ± standard deviation (SD). $^{*}P<0.05$, $^{**}P<0.01$, $^{***}P<0.001$; n.s. no significant; $n=3$; **h** specimens of the spinal cords of all experimental groups 12 weeks postsurgery; the black rectangles indicate the lesion sites

which provided electrophysiological evidence for motor function recovery attributed to AFGN-NSC implantation.

At 12 weeks postsurgery, the physical tissue repair of the spinal cord and bladder was also evaluated. As shown in Fig. 2h, the lesion epicenters of the spinal cord tissue in the control and NSC groups remained empty. In the AFGN group, the gaps were partially filled by the newly regenerated tissues with rough and irregular surfaces, whereas those in the AFGN-NSC group almost occupied the majority of the lesion sites and presented good integration with the host spinal cord.

Neurogenic bladder is one of the most fatal complications of SCI [53]. Therefore, the protection and repair of bladder tissue is a therapeutic challenge during SCI recovery. We found that the enhanced regeneration of the spinal cord in the AFGN-NSC group displayed a synergistic benefit for the protection and recovery of bladder tissue (Fig. S7). In the control group, the bladder wall exhibited severe thickening and fibrosis changes, along with muscle atrophy and edema of the mucous membrane. However, the pathological damage of the bladder tissue was successfully restricted in the AFGN-NSC group. These results, combined with BBB, CatWalk, and electrophysiological evaluations, demonstrated that the grafted NSCs carried by the AFGN hydrogel improved tissue repair and functional recovery after SCI. In addition, the H&E staining images of the hearts, livers, spleens, kidneys, and lungs exhibited no obvious cellular toxicity and pathological differences in any of the groups (Fig. S8), which demonstrated reliable biocompatibility of the implanted NSCs and AFGN hydrogel [54].

Delivery of NSCs via the AFGN Hydrogel Regulates the Local Immune Environment and Reduces Inflammation-Triggered Secondary Injury

The spinal cord tissue sections were further examined to confirm the function of the AFGN hydrogel-NSC system in promoting SCI repair and functional recovery. The neuroinflammation induced by recruited macrophages is well documented to reach a peak at the lesion site 7 days after acute SCI, resulting in a cascade of secondary injury processes [55]. Activated macrophages can bind to specific factors and polarize into the M1 subtype (exert proinflammatory function) and M2 subtype (exert anti-inflammatory function). To examine the effect of AFGN-NSC transplantation on inflammatory regulation, immunostaining for CD68 (a marker of activated macrophages) and CD206 (a marker of M2 macrophages) was performed 7 days after injury. We found that abundant activated macrophages accumulated at the lesion site (Fig. 3a), while treatment with AFGN or AFGN-NSC noticeably reduced the number of activated macrophages and presented large quantities of M2 macrophages in the injured area compared with the other groups ($P < 0.001$ for AFGN-NSC vs. control and NSC, respectively; n.s. for AFGN-NSC vs. AFGN) (Fig. 3a, b). However, there was no statistical difference between the AFGN and AFGN-NSC group in the inhibitory effect on inflammation. The results of qRT-PCR in vitro showed a similar trend as immunostaining (Fig. S9). The expression of inflammatory gene Iba1 in the TCP control group was significantly higher than other groups. The expression of proinflammatory genes TNF-α and CD86 in the AFGN group decreased obviously when compared with other groups, but the expression of TNF-α showed no statistical difference between the TCP control and NSC group. Moreover, compared with the other two groups, the expression of anti-inflammatory gene Arg-1 showed a significantly upward trend in the AFGN group. These results could be explained by the fact that the AFGN hydrogel could exert immunomodulation function to regulate the infiltration of macrophages and shift activated macrophages into the M2 subtype even without NSCs, possibly due to its suitable physicochemical properties and the nanostructure–function relationship, in agreement with the previous studies [56–58]. It is notable that the NSCs also had a certain degree of alleviating inflammation both in vivo and in vitro, which might be due to the complex crosstalk between the activated macrophages and the various cytokines secreted by NSCs [59].

The acute inflammatory storm induced by activated M1 macrophages after SCI can cause syringomyelia and trigger reactive scar-forming astrocytes to deposit axon-inhibitory chondroitin sulfate proteoglycan (CSPG) [24, 60], leading to the formation of glial scars and chronic failure of axon regeneration. As shown in H&E staining images (Fig. 3c), dense glial scars and obvious cavities were found in the control group. In the NSC group, a few regeneration tissues randomly grew into the SCI area. Without the mechanical support of the scaffold, grafted NSCs have previously been shown to tend to spread into the surfaces of surrounding tissue as a result of the incongruousness in mechanical strength [61]. Moreover, without the shelter created by the scaffold, the grafted NSCs were directly exposed to the hostile niche, in which the infiltrated macrophages could secrete cytotoxic factors to attack foreign bodies [62–64]. These processes may cause the loss and apoptosis of grafted NSCs, resulting in the formation of glial scars and cavities that are similar to those in the control group [61]. In the AFGN and AFGN-NSC groups, many newborn tissues permeated into the injured site with a scaffold-oriented aligned direction. On the other hand, the mean volume of cavities was significantly reduced in the AFGN-NSC group compared to the other groups ($P < 0.001$ for AFGN-NSC vs. control and NSC, respectively; $P < 0.01$ for AFGN-NSC vs. AFGN) (Fig. 3c, d). Moreover, we performed immunostaining for CS-56 (a marker of CSPG) to assess CSPG deposition 12 weeks after SCI. In the control group, obvious CSPG deposition with a wall-like structure filled the epicenter of the lesion site

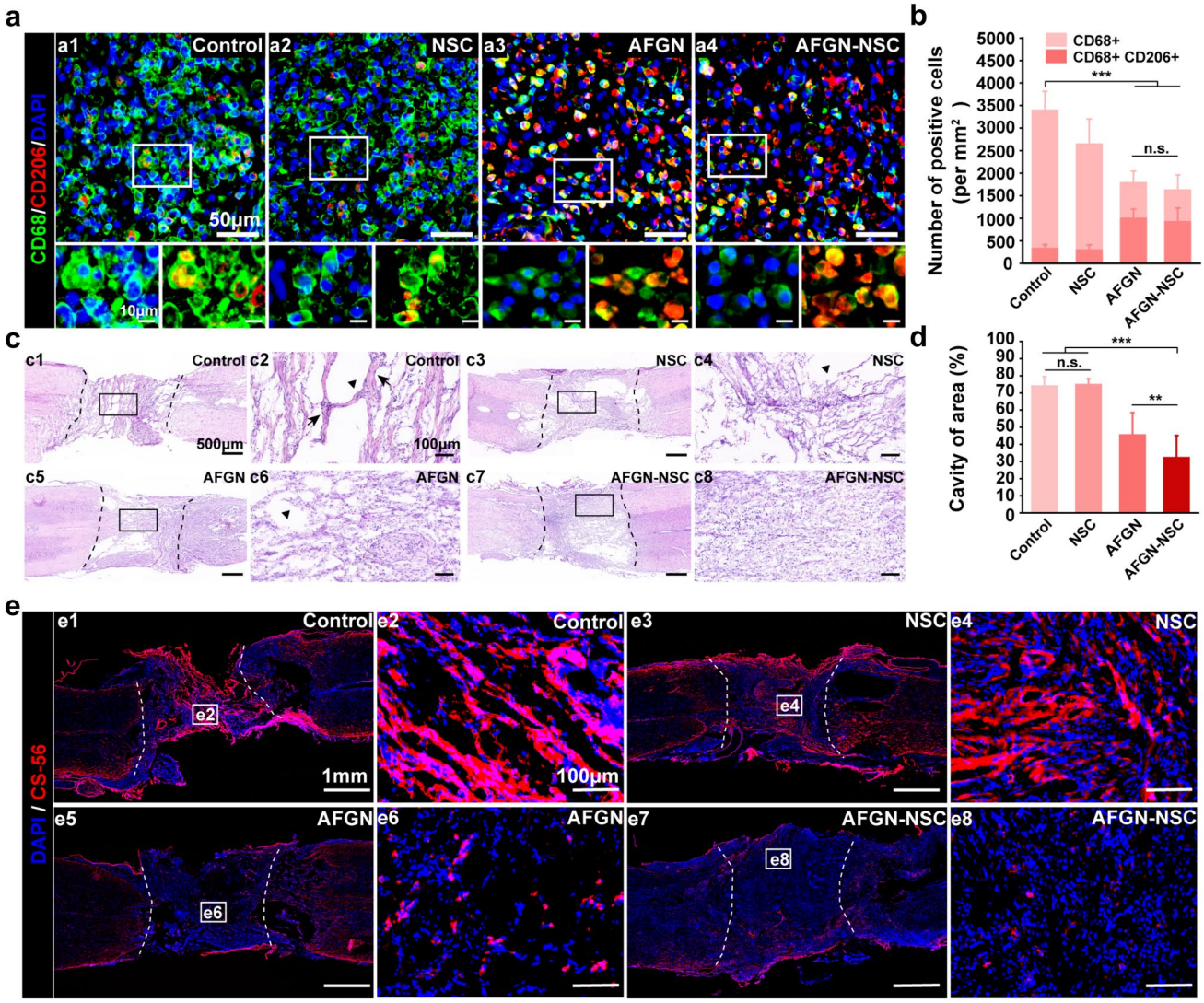

Fig. 3 Modulation of local inflammatory response and inflammation-triggered secondary injury. **a** Representative images of CD68 (green)/CD206 (red)/DAPI (blue) immunostaining at the lesion site and the amplified images of each group at 1 week postgrafting. **b** Quantification of the density of CD68-positive and CD68/CD206 dual-positive cells. $***P<0.001$; $n=5$, **c** Representative images of H&E staining (nuclei: blue, cytoplasm: red) for longitudinal sections of each group, 4 weeks postgrafting, **c2**, **c4, c6, c8** Enlarged images from **c1, c3, c5, c7**, respectively; the dotted lines indicate the boundaries between the lesion site and the host spinal cord; the black triangles indicate cavity formation; the black arrows indicate glial scar, **d** Quantification of the cavity of area (cavity area/total area). Data are presented as the mean ± (SD); $**P<0.01$, $***P<0.001$; n.s. no significant; $n=5$, **e** Representative immunostaining images of CS-56 from different treatment groups 12 weeks postsurgery, **e2, e4, e6, e8** The enlarged images of the boxed regions in **e1, e3, e5, e7**, respectively; the dotted lines indicate the boundaries between the lesion site and the host tissue

and surrounded the lesion boundary. Conversely, only sporadic CSPG deposition was found in the AFGN-NSC group (Fig. 3e). Collectively, our results suggest that the AFGN hydrogel in combination with NSCs regulates the local neuroinflammation niche by shifting activated macrophages into the M2 subtype after acute SCI. The modified early stage immune microenvironment further alleviated syringomyelia and reduced the deposition of CSPG at the lesion site, achieving a long-term effect on mitigating the formation of glial scars in scenarios of secondary injury processes, paving the way for SCI repair.

The AFGN Exerts NSC-Protective Effects and Directed Neuronal Differentiation of Grafted NSCs

The inhospitable niche at the lesion site after SCI and the lack of adhesive cues cause low-grafted NSC retention and neuronal differentiation but facilitate glial lineage

differentiation, which constitutes the main barrier to NSC-based SCI therapies [4–6]. To investigate whether the AFGN could induce NSC retention and neuronal differentiation in vivo in the middle stage of SCI, immunostaining of Tuj-1, GFAP, and GFP were used to label newborn neurons, astrocytes, and grafted NSCs, respectively (Fig. 4a). Four weeks postgrafting, abundant GFP-positive NSCs were detected at the lesion site in the AFGN-NSC group, effectively preventing the loss of grafted NSCs (Fig. 4a1). Conversely, the grafted NSC density (ratio of GFP-positive area to total area) in the NSC group was significantly decreased ($P < 0.001$) (Fig. 4a2, b). Meanwhile, the AFGN-NSC group exhibited a significantly higher fraction of GFP/Tuj-1 double-positive area as well as a lower fraction of GFP/GFAP double-positive area than the NSC group ($P < 0.001$) (Fig. 4a1, a2, c), indicating that the AFGN hydrogel could promote the neuronal differentiation of grafted NSCs and inhibit glial differentiation. Moreover, the AFGN-NSC group remarkably boosted Tuj-1-labeled neuron regeneration manifesting tubules in the central lesion compared with other groups ($P < 0.01$) (Fig. 4a, d). These results could be explained by the fact that the NCAD could enhance the

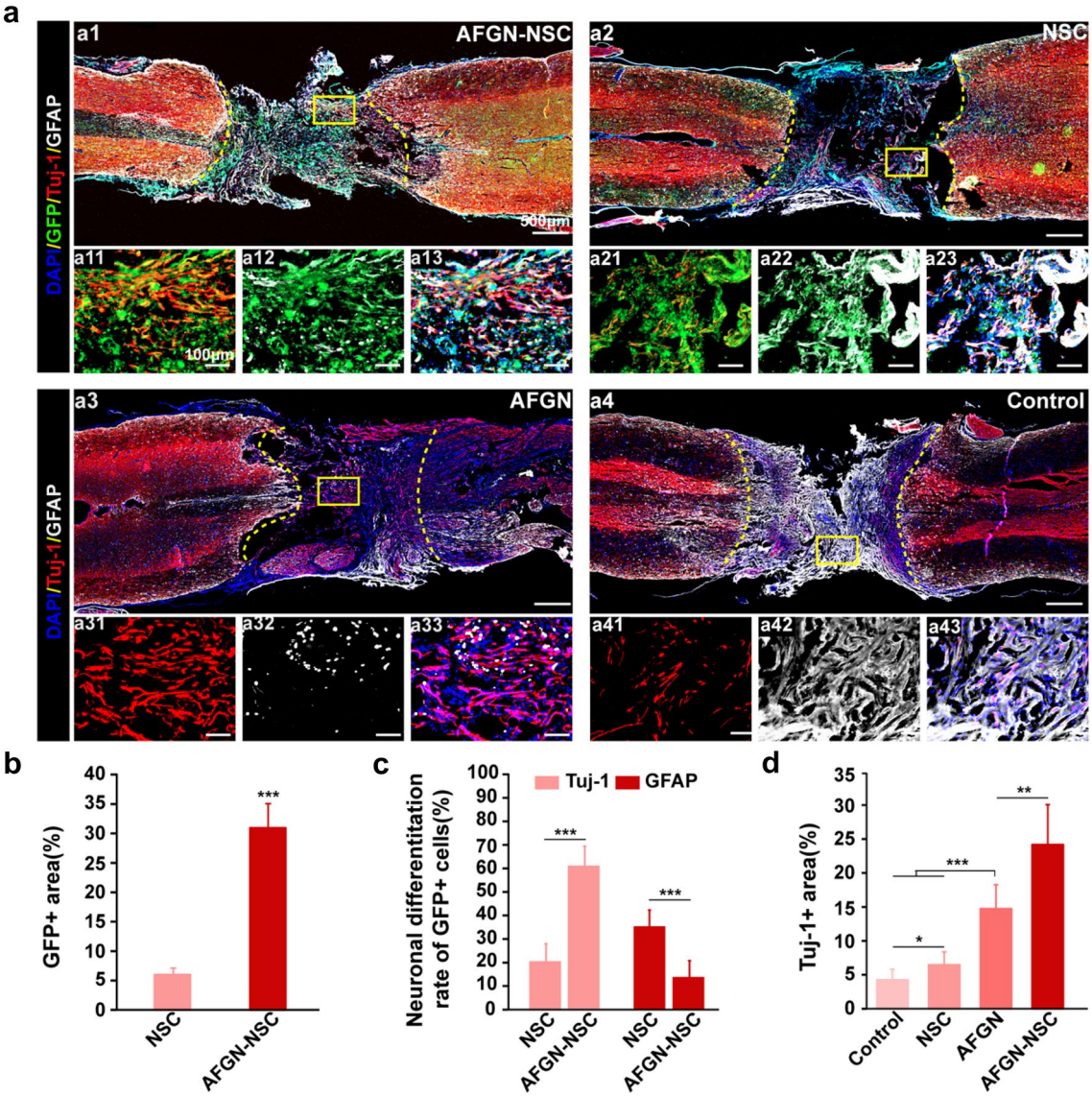

Fig. 4 Retention and neuronal differentiation of grafted NSCs and neural regeneration. **a** Representative images of Tuj-1 (red), GFAP (white), and DAPI (blue) immunostaining for longitudinal sections of each group at 4 weeks postgrafting. The implanted NSCs are identified by GFP fluorescence signals (green) in **a3–a4**. **a11–a13, a21–a23, a31–a33, a41–a43** Enlarged images from **a1, a2, a3, a4,** respectively, **b** quantification of GFP-positive area from the enlarged view, **c** quantitative analysis of the GFP/Tuj-1 and GFP/GFAP dual-positive area from the enlarged view, and **d** quantification of Tuj-1-positive area from the enlarged view. Data are presented as the mean ± (SD); $^{*}P < 0.05$, $^{**}P < 0.01$, $^{***}P < 0.001$; $n = 5$

mechanotransduction of the cell–biomaterial interface and mediate NSCs to better perceive the biophysical cues generated by the AFGN hydrogel, leading to an enhancement retention of grafted NSCs in the lesion site through the cell–biomaterial and cell–cell adhesive contacts [27, 28, 30, 31]. In addition, previous studies have shown that NCAD can also exert biochemical cues to reduce the level of cytoplasmic β-catenin, which promotes the neural differentiation of grafted NSCs through the Wnt/β-catenin and AKT signaling pathways [34, 35]. Taken together, the AFGN hydrogel could significantly promote adhesion and neural differentiation of grafted NSCs in the SCI area, demonstrating an efficient desirable niche reconstruction capacity of the AFGN hydrogel.

NSC Delivery via the AFGN Hydrogel Facilitates Angiogenesis and Axon Remyelination

The process of angiogenesis after SCI is essential for axonal regeneration and long-term survival, because it is crucial for the supply of nutrients and oxygen [65]. To better evaluate the vascularization effects of the AFGN hydrogel loaded with NSCs, we performed immunostaining for Tuj-1 and RECA-1 (a marker of vascular endothelial cells) 8 weeks after SCI (Fig. 5a). Only a few sporadic Tuj-1- and RECA-1-labeled cells could be seen at the lesion site in the control group and the NSC group (Fig. 5a1, a2). In contrast, the AFGN group exhibited enhanced neurogenesis accompanied by balanced vascularization (Fig. 5a3), which may be due to NCAD-induced neurite outgrowth [66] and the capacity of fibrin to promote endothelial cells to form functional vasculature [65]. Notably, the AFGN-NSC group promoted a significantly larger number of Tuj-1-labeled regrowth axons in directional arrangement synergizing with RECA-1-labeled lumen-like matured vessel structures, which were more obvious than those in the AFGN group (Fig. 5a3, a4). These findings suggest that the NSCs in the AFGN hydrogel might exert paracrine effects and synergize with the scaffold, providing a hospitable microenvironment for long-term axon regeneration and vascularization after SCI [67].

The myelin sheath is required for normal axon development and maintenance and plays a critical role in supplying axon-needed nutrition and accelerating axonal signal conduction [68]. The regenerated tissues in all groups were harvested and sliced transversely at the epicenter of the lesion site for the evaluation of axon regeneration and remyelination 12 weeks after SCI. The toluidine blue staining images revealed many regrowing axons wrapped in myelin sheaths in the AFGN-NSC group. In comparison, such structures were much less prevalent in the AFGN group and sporadically appeared in the NSC and control groups (Fig. 5b). Quantitative analysis suggested that both the density of nerve fibers and myelinated nerve fibers were significantly higher in the AFGN-NSC group than in the other three groups ($P < 0.001$), approaching those of normal spinal cord tissue but with a significant difference ($P < 0.001$) (Fig. 5c, d). Furthermore, TEM images were used to examine the ultrastructural details of the myelin sheath, including the myelin sheath thickness and myelinated axon area. In the AFGN-NSC group, the myelin sheath was significantly thicker than those in the other three groups ($P < 0.01$), and the area-based G-ratio (axon area/whole myelinated axon area) was significantly lower than those in the other three groups ($P < 0.05$); in both cases, the values in the AFGN-NSC group were closest to those in normal spinal cord tissue but with significant differences (Fig. 5e, f). Moreover, the structure of myelin sheath-wrapped axons evaluated by immunofluorescence for neurofilament 200 (NF, a marker of mature neurons)/myelin basic protein (MBP, a marker of myelin sheath) was also more obvious in the AFGN-NSC group compared with other groups (Fig. 5g and S10), which is consistent with the previous results. Taken together, these results indicate remarkable axon regeneration and mature myelin regeneration mediated by the synergistic effect of the AFGN hydrogel and grafted NSCs, verifying the previously reported mechanisms of the initial axon–oligodendrocyte contact myelination process and NSC systematic differentiation induced by NCAD [26, 69, 70].

Delivery of NSCs via the AFGN Hydrogel Promotes Neural Relay Formation and Functional Neurons' Regeneration

The transplanted exogenous NSCs could differentiate into neurons and form synaptic connections with host neurons at the lesion site, which is considered to be crucial for neural relay reconstruction and functional recovery after SCI [71]. To investigate the long-term fate of grafted NSCs, immunostaining for GFP, NF, and SYN was used to visualize grafted NSCs, neurofilaments (a marker of mature neurons), and synapses, respectively (Fig. 6a), at 12 weeks postsurgery. The immunostaining results showed that the AFGN-NSC group remarkably boost directional neurofilament regeneration at the lesion site (Fig. 6a4), which was of great significant superiority compared with other groups ($P < 0.001$) (Fig. 6a, b). In the AFGN-NSC group, many GFP-positive NSCs were evenly dispersed at the lesion site and migrated into the adjacent host spinal cord tissue. Moreover, high-density GFP and NF double-positive signals were also observed both in the injured area and adjacent host tissue (Fig. 6a4). However, in the NSC group, such positive signals were greatly attenuated in the absence of the AFGN hydrogel ($P < 0.001$) (Fig. 6a3, c). These results demonstrate that the AFGN hydrogel could provide a favorable niche for the implanted NSCs and continuously exert differentiation

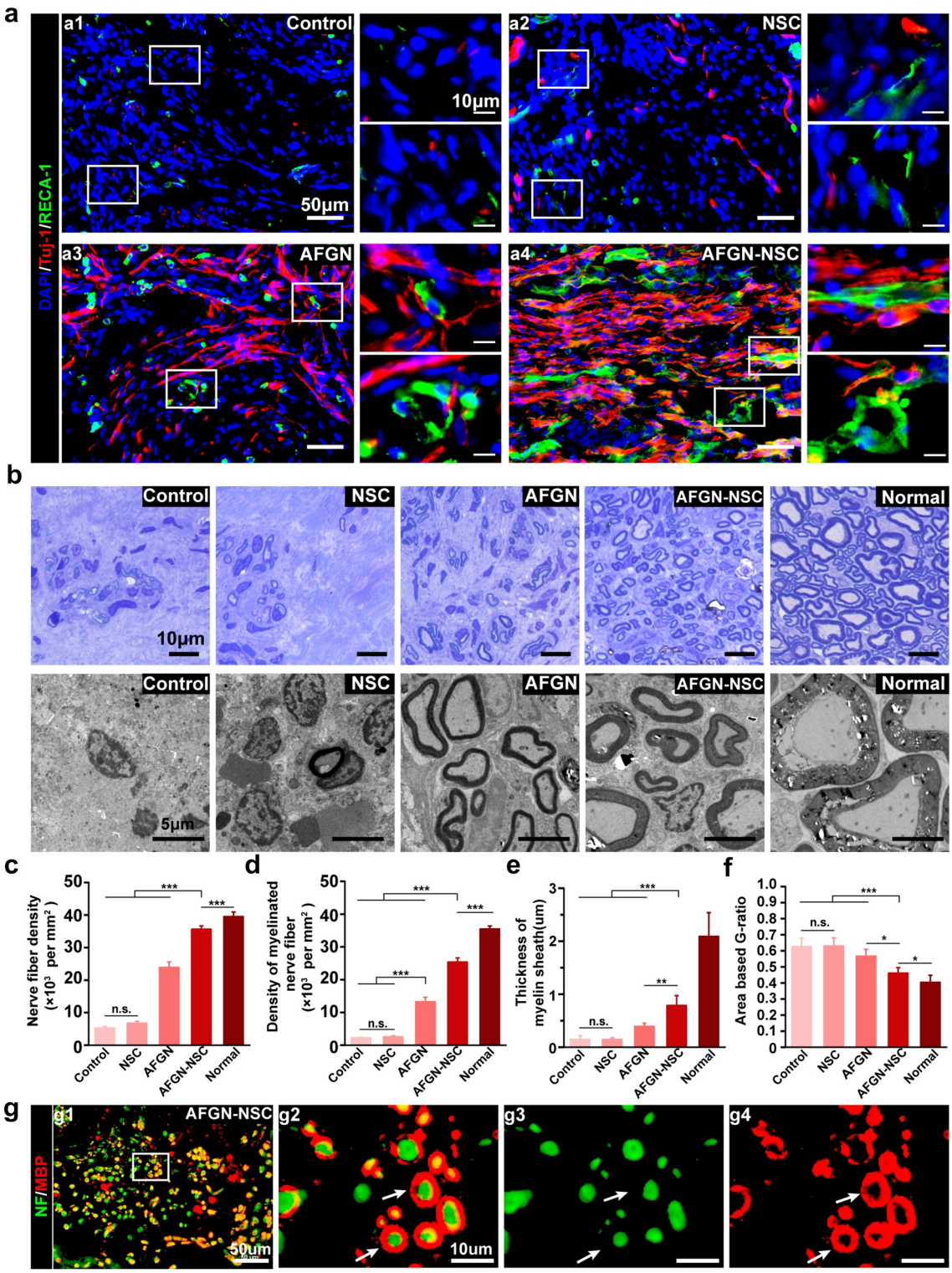

Fig. 5 Revascularization and axonal remyelination. **a** Representative images of Tuj-1 (red)/RECA-1 (green)/DAPI (blue) immunostaining at the lesion site of each group at 12 weeks postgrafting, **b** representative toluidine blue staining and TEM images of regenerated myelin in uninjured sites and the lesion core of the control, NSC, AFGN, and AFGN-NSC groups at 12 weeks postgrafting, **c** quantitative analysis of the density of nerve fibers from toluidine blue staining images, **d** quantitative analysis of the density of myelinated nerve fibers from toluidine blue staining images, **e** quantitative analysis of the myelin sheath from TEM images, and **f** quantitative analysis of the area-based G-ratio from TEM images. $^{*}P<0.05$, $^{**}P<0.01$, $^{***}P<0.001$; n.s. no significant; $n=3$; **g** representative images of NF (green)/MBP (red) immunostaining at the lesion core of the AFGN-NSC group at 12 weeks postgrafting, **g2–g4** Enlarged images from **g1**

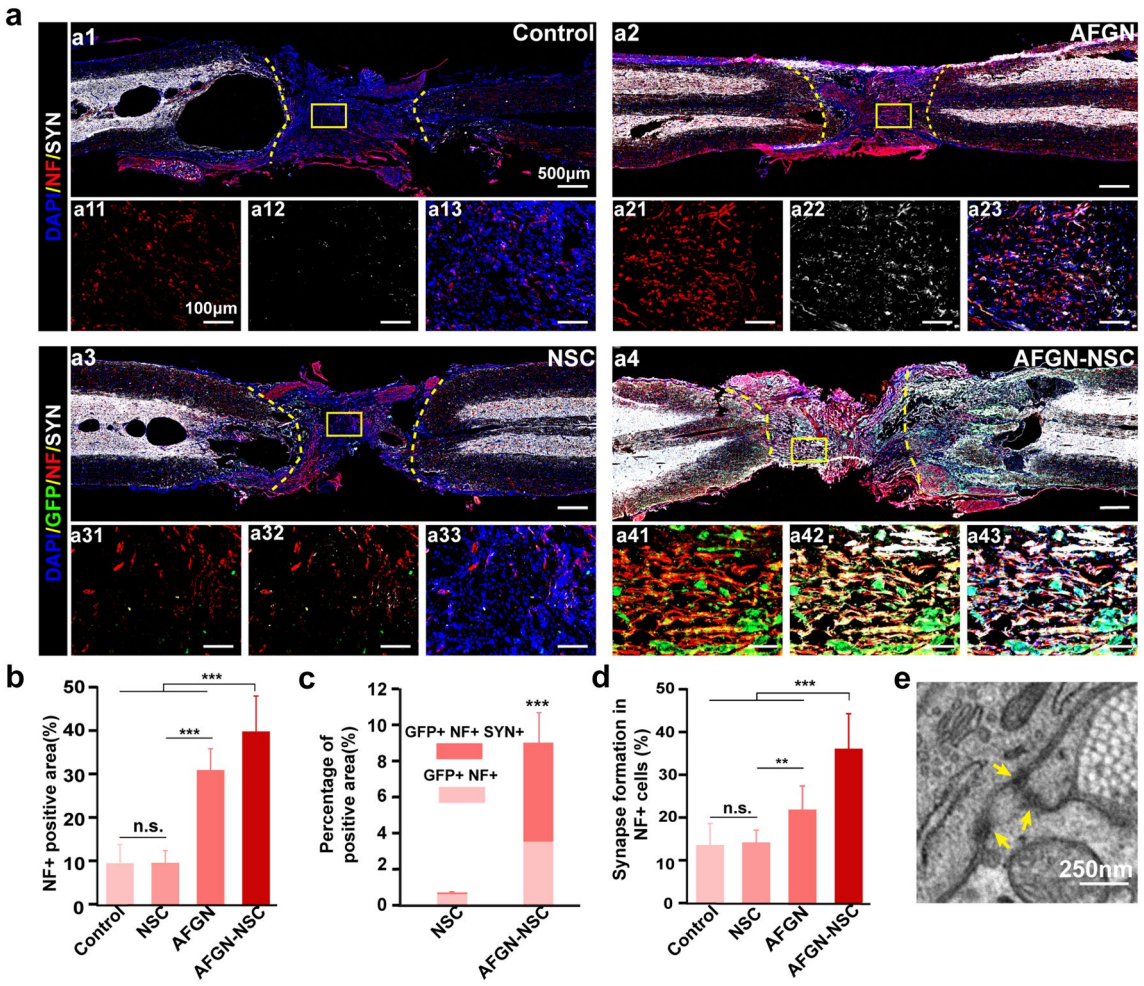

Fig. 6 Neural relay formation. **a** Representative images of NF (red), SYN (white), and DAPI (blue) immunostaining for longitudinal sections of each group at 12 weeks postgrafting. The implanted NSCs are identified by GFP fluorescence signals (green) in **a3–a4**; **a11–a13, a21–a23, a31–a33, a41–a43** Enlarged images from **a1, a2, a3, a4**, respectively, **b** Quantitative analysis of the NF-positive area from the enlarged view, **c** Quantitative analysis of the GFP/NF and GFP/NF/SYN copositive area from the enlarged view, **d** Quantitative analysis of the NF/SYN dual-positive area from the enlarged view. Data are presented as the mean ± (SD); $^{**}P < 0.01$, $^{***}P < 0.001$; n.s. no significant difference; $n = 5$, **e** TEM images of the synapses at the lesion core in the AFGN-NSC group; the yellow arrows indicate the ultrastructure of synapses

information for the regeneration of nerve fibers derived from the grafted NSCs.

Moreover, in the AFGN-NSC group, many NF-positive neurofilaments migrated from the lesion boundary into the injured area and were in dense contact with GFP/NF-copositive neurofilaments (Fig. 6a4). Copositive immunofluorescence signals of GFP/NF/SYN and NF/SYN indicated abundant newly formed synapses between the grafted NSC-derived neurons and newly regenerated host axons in the AFGN-NSC group, which revealed a significant difference compared with other groups ($P < 0.001$) (Fig. 6a, d). The existence of reconstructed synapses was also confirmed by TEM (Fig. 6e). In addition, the AFGN-NSC group exhibited significant functional nerve fibers regeneration at the lesion site, including GFP/NF/tyrosine hydroxylase (TH) copositive nerve fibers (Fig. S11a) and GFP/NF/5-hydroxytryptamine (5-HT) copositive nerve fibers (Fig. S11b). This finding indicated partial NSC-derived neuronal differentiation into motor functional neurons and the restoration of nerve circuits [47, 71, 72]. These results demonstrated that the synergistic action of AFGN hydrogel loaded with NSCs induced neuron regeneration, neural relay formation, and nerve circuit reconstruction when transplanted after SCI. Additionally, the effects of the separate AFGN hydrogel and exogenous NSC implantation were also examined and showed relatively limited improvement in neural repair. The AFGN hydrogel could exert biophysical and biochemical cues to guarantee that implanted NSCs are evenly retained in a favorable niche and differentiate into neurons for a long time, provide directional guidance to the implanted NSCs

and regenerated neurons, and enhance the efficiency of the functional integration between exogenous NSC-derived interneurons and host neurons, paving the way for the formation of correct synaptic connections and nerve circuit reconstruction [73, 74]. Moreover, NCAD could mediate synaptic adhesion by regulating the level of α-amino-3-hydroxy-5-methyl-4-isoxazole propionic acid in the postsynaptic region, which could further enhance synaptic plasticity and stability [75], contributing to functional recovery.

Overall, compared to the previous scaffold-based NSC transplantation strategy, we orchestrated the advantages of the nanostructure presented by fibrin-based scaffold and the biochemical effects of NCAD-Fc to determine cell fate of delivered NSCs in a favorable niche, proposing an effective combinatorial therapy in SCI repair.

Conclusions

In summary, we designed and fabricated an NCAD-functionalized aligned fibrin nanofiber hydrogel that provided both biophysical and biochemical cues as a superior niche for the delivery and regulation of exogenous NSCs. The AFGN hydrogel could significantly promote the adhesion and neuronal differentiation of NSCs *via* enhanced cell–cell communication and cell–biomaterial interactions. More importantly, the AFGN exhibited an outstanding capacity for reconstructing favorable niche to effectively promote the long-term preservation, integration, and cell fate regulation of implanted NSCs *in vivo*. In addition, the NSCs-loaded AFGN that was implanted in a rat 2 mm-long complete transected SCI model significantly reduced the inflammatory response and glial scar formation, boosted neurogenesis and vascularization, and achieved good neural relay and nerve circuit restoration, thus contributing to encouraging locomotor functional recovery after SCI. This study presents a promising combinatorial therapy to treat acute SCI, which may provide new perspectives for future neural tissue engineering designs. Future studies are necessary to verify the effects of AFGN-NSC transplantation therapy in a nonhuman primate SCI model to provide more solid evidence for clinical translation.

Supplementary Information The online version contains supplementary material available at https://doi.org/10.1007/s42765-023-00272-w.

Acknowledgements We thank Kumiko Matsunaga and colleagues from SOMAR (Japan) Corporation Biomaterials Dept. for the help of N-cadherin-Fc preparation. We thank Kumiko Matsunaga from SOMAR (Japan) Corp. and Jun Liu from Tsinghua University for the help of research materials transportation. We thank Professor Li-Na Zhang from Central South University for the help of rat HAPI microglia cells preparation and transportation. We also thank Yue-teng Wei from Bruker Corp. for the help of atomic force microscope operation. Schemes and Table of Contents (TOC) are created with BioRender.com. This work was financially supported by the National Natural Science Foundation of China (Grant Nos. 32271414 and 82201521), the Tsinghua Precision Medicine Foundation (Grant No. 2022TS001), and the National Key Research and Development Program of China (Grant No. 2020YFC1107600).

Data availability The data that support the findings of this study are available from the corresponding author upon reasonable request.

Declarations

Conflict of Interest The authors declare that there are no conflicts of interest.

References

1. Jazayeri SB, Beygi S, Shokraneh F, Hagen EM, Rahimi-Movaghar V. Incidence of traumatic spinal cord injury worldwide: a systematic review. *Eur Spine J*. **2015**;*24*:905.
2. Fischer I, Dulin JN, Lane MA. Transplanting neural progenitor cells to restore connectivity after spinal cord injury. *Nat Rev Neurosci*. **2020**;*21*:366.
3. Lu P, Wang Y, Graham L, McHale K, Gao M, Wu D, Brock J, Blesch A, Rosenzweig ES, Havton LA, Zheng B, Conner JM, Marsala M, Tuszynski MH. Long-distance growth and connectivity of neural stem cells after severe spinal cord injury. *Cell*. **2012**;*150*:1264.
4. Buddensiek J, Dressel A, Kowalski M, Storch A, Sabolek M. Adult cerebrospinal fluid inhibits neurogenesis but facilitates gliogenesis from fetal rat neural stem cells. *J Neurosci Res*. **2009**;*87*:3054.
5. Deng W, Shao F, He Q, Wang Q, Shi W, Yu Q, Cao X, Feng C, Bi S, Chen J, Ma P, Li Y, Gong A, Tong S, Yu J, Spector M, Xu X, Zhang Z. EMSCs build an all-in-one niche via cell-cell lipid raft assembly for promoted neuronal but suppressed astroglial differentiation of neural stem cells. *Adv Mater*. **2019**;*31*: e1806861.
6. Xu B, Zhao Y, Xiao Z, Wang B, Liang H, Li X, Fang Y, Han S, Li X, Fan C, Dai J. A dual functional scaffold tethered with EGFR antibody promotes neural stem cell retention and neuronal differentiation for spinal cord injury repair. *Adv Healthc Mater*. **2017**. https://doi.org/10.1002/adhm.201601279.
7. Liu Z, Wan X, Wang ZL, Li L. Electroactive biomaterials and systems for cell fate determination and tissue regeneration: design and applications. *Adv Mater*. **2021**;*33*: e2007429.

8. Matta R, Gonzalez AL. Engineered biomimetic neural stem cell niche. *Curr Stem Cell Rep*. **2019**;*5*:109.
9. Alvarez Z, Kolberg-Edelbrock AN, Sasselli IR, Ortega JA, Qiu R, Syrgiannis Z, Mirau PA, Chen F, Chin SM, Weigand S, Kiskinis E, Stupp SI. Bioactive scaffolds with enhanced supramolecular motion promote recovery from spinal cord injury. *Science*. **2021**;*374*:848.
10. Yao S, Yu S, Cao Z, Yang Y, Yu X, Mao HQ, Wang LN, Sun X, Zhao L, Wang X. Hierarchically aligned fibrin nanofiber hydrogel accelerated axonal regrowth and locomotor function recovery in rat spinal cord injury. *Int J Nanomed*. **2018**;*13*:2883.
11. Liu W, Xu B, Xue W, Yang B, Fan Y, Chen B, Xiao Z, Xue X, Sun Z, Shu M, Zhang Q, Shi Y, Zhao Y, Dai J. A functional scaffold to promote the migration and neuronal differentiation of neural stem/progenitor cells for spinal cord injury repair. *Biomaterials*. **2020**;*243*: 119941.
12. Sever-Bahcekapili M, Yilmaz C, Demirel A, Kilinc MC, Dogan I, Caglar YS, Guler MO, Tekinay AB. Neuroactive peptide nanofibers for regeneration of spinal cord after injury. *Macromol Biosci*. **2021**;*21*: e2000234.
13. Rao JS, Zhao C, Zhang A, Duan H, Hao P, Wei RH, Shang J, Zhao W, Liu Z, Yu J, Fan KS, Tian Z, He Q, Song W, Yang Z, Sun YE, Li X. NT3-chitosan enables de novo regeneration and functional recovery in monkeys after spinal cord injury. *Proc Natl Acad Sci USA*. **2018**;*115*:E5595.
14. Yao S, He F, Cao Z, Sun Z, Chen Y, Zhao H, Yu X, Wang X, Yang Y, Rosei F, Wang LN. Mesenchymal stem cell-laden hydrogel microfibers for promoting nerve fiber regeneration in long-distance spinal cord transection injury. *ACS Biomater Sci Eng*. **2020**;*6*:1165.
15. Wan XY, Liu ZR, Li LL. Manipulation of stem cells fates: the master and multifaceted roles of biophysical cues of biomaterials. *Adv Funct Mater*. **2021**. https://doi.org/10.1002/adfm.202010626.
16. Zhang X, Cui X, Wang D, Wang S, Liu Z, Zhao G, Zhang Y, Li Z, Wang ZL, Li L. Piezoelectric nanotopography induced neuron-like differentiation of stem cells. *Adv Funct Mater*. **2019**. https://doi.org/10.1002/adfm.201900372.
17. Spotnitz WD. Fibrin sealant: past, present, and future: a brief review. *World J Surg*. **2010**;*34*:632.
18. Yu Z, Li H, Xia P, Kong W, Chang Y, Fu C, Wang K, Yang X, Qi Z. Application of fibrin-based hydrogels for nerve protection and regeneration after spinal cord injury. *J Biol Eng*. **2020**;*14*:22.
19. Brown AC, Barker TH. Fibrin-based biomaterials: modulation of macroscopic properties through rational design at the molecular level. *Acta Biomater*. **2014**;*10*:1502.
20. King VR, Alovskaya A, Wei DY, Brown RA, Priestley JV. The use of injectable forms of fibrin and fibronectin to support axonal ingrowth after spinal cord injury. *Biomaterials*. **2010**;*31*:4447.
21. Chen Z, Zhang H, Fan C, Zhuang Y, Yang W, Chen Y, Shen H, Xiao Z, Zhao Y, Li X, Dai J. Adhesive, stretchable, and spatiotemporal delivery fibrous hydrogels harness endogenous neural stem/progenitor cells for spinal cord injury repair. *ACS Nano*. **1986**;*2022*:16.
22. Yao S, Liu X, Yu S, Wang X, Zhang S, Wu Q, Sun X, Mao H. Co-effects of matrix low elasticity and aligned topography on stem cell neurogenic differentiation and rapid neurite outgrowth. *Nanoscale*. **2016**;*8*:10252.
23. Cao Z, Yao S, Xiong Y, Zhang Z, Yang Y, He F, Zhao H, Guo Y, Wang G, Xie S, Guo H, Wang X. Directional axonal regrowth induced by an aligned fibrin nanofiber hydrogel contributes to improved motor function recovery in canine L2 spinal cord injury. *J Mater Sci Mater Med*. **2020**;*31*:40.
24. Man W, Yang S, Cao Z, Lu J, Kong X, Sun X, Zhao L, Guo Y, Yao S, Wang G, Wang X. A multi-modal delivery strategy for spinal cord regeneration using a composite hydrogel presenting biophysical and biochemical cues synergistically. *Biomaterials*. **2021**;*276*: 120971.
25. Zhang Y, Qin Z, Qu ZY, Ge M, Yang J. Cadherin-based biomaterials: inducing stem cell fate towards tissue construction and therapeutics. *Progress Nat Sci-Mater Int*. **2020**;*30*:597.
26. Chooi WH, Chew SY. Modulation of cell-cell interactions for neural tissue engineering: potential therapeutic applications of cell adhesion molecules in nerve regeneration. *Biomaterials*. **2019**;*197*:327.
27. Takeichi M. The cadherin superfamily in neuronal connections and interactions. *Nat Rev Neurosci*. **2007**;*8*:11.
28. Hong E, Brewster R. N-cadherin is required for the polarized cell behaviors that drive neurulation in the zebrafish. *Development*. **2006**;*133*:3895.
29. Liu Z, Cai M, Zhang X, Yu X, Wang S, Wan X, Wang ZL, Li L. Cell-traction-triggered on-demand electrical stimulation for neuron-like differentiation. *Adv Mater*. **2021**;*33*: e2106317.
30. Nelson WJ, Weis WI. 25 years of tension over actin binding to the cadherin cell adhesion complex: the devil is in the details. *Trends Cell Biol*. **2016**;*26*:471.
31. Vega LJ, Lee MK, Jeong JH, Smith CE, Lee KY, Chung HJ, Leckband DE, Kong H. Recapitulating cell-cell adhesion using N-cadherin biologically tethered to substrates. *Biomacromol*. **2014**;*15*:2172.
32. Utton MA, Eickholt B, Howell FV, Wallis J, Doherty P. Soluble N-cadherin stimulates fibroblast growth factor receptor dependent neurite outgrowth and N-cadherin and the fibroblast growth factor receptor co-cluster in cells. *J Neurochem*. **2001**;*76*:1421.
33. Miyamoto Y, Sakane F, Hashimoto K. N-cadherin-based adherens junction regulates the maintenance, proliferation, and differentiation of neural progenitor cells during development. *Cell Adh Migr*. **2015**;*9*:183.
34. Maher MT, Flozak AS, Stocker AM, Chenn A, Gottardi CJ. Activity of the beta-catenin phosphodestruction complex at cell-cell contacts is enhanced by cadherin-based adhesion. *J Cell Biol*. **2009**;*186*:219.
35. Zhang J, Shemezis JR, McQuinn ER, Wang J, Sverdlov M, Chenn A. AKT activation by N-cadherin regulates beta-catenin signaling and neuronal differentiation during cortical development. *Neural Dev*. **2013**;*8*:7.
36. Yue XS, Murakami Y, Tamai T, Nagaoka M, Cho CS, Ito Y, Akaike T. A fusion protein N-cadherin-Fc as an artificial extracellular matrix surface for maintenance of stem cell features. *Biomaterials*. **2010**;*31*:5287.
37. Czajkowsky DM, Hu J, Shao Z, Pleass RJ. Fc-fusion proteins: new developments and future perspectives. *EMBO Mol Med*. **2012**;*4*:1015.
38. Cherry JF, Bennett NK, Schachner M, Moghe PV. Engineered N-cadherin and L1 biomimetic substrates concertedly promote neuronal differentiation, neurite extension and neuroprotection of human neural stem cells. *Acta Biomater*. **2014**;*10*:4113.
39. Vega LJ, Lee MK, Qin EC, Rich M, Lee KY, Kim DH, Chung HJ, Leckband DE, Kong H. Three dimensional conjugation of recombinant N-cadherin to a hydrogel for in vitro anisotropic neural growth. *J Mater Chem B*. **2016**;*4*:6803.
40. Qazi TH, Mooney DJ, Duda GN, Geissler S. Biomaterials that promote cell-cell interactions enhance the paracrine function of MSCs. *Biomaterials*. **2017**;*140*:103.

41. Osathanon T, Giachelli CM, Somerman MJ. Immobilization of alkaline phosphatase on microporous nanofibrous fibrin scaffolds for bone tissue engineering. *Biomaterials*. **2009**;*30*:4513.
42. Karageorgiou V, Meinel L, Hofmann S, Malhotra A, Volloch V, Kaplan D. Bone morphogenetic protein-2 decorated silk fibroin films induce osteogenic differentiation of human bone marrow stromal cells. *J Biomed Mater Res A*. **2004**;*71*:528.
43. Xu K, Zhu C, Xie J, Li X, Zhang Y, Yao F, Gu Z, Yang J. Enhanced vascularization of PCL porous scaffolds through VEGF-Fc modification. *J Mater Chem B*. **2018**;*6*:4474.
44. Mehwish N, Dou X, Zhao C, Feng C, Fu Q. Chirality transfer in supramolecular co-assembled fibrous material enabling the visual recognition of sucrose. *Adv Fiber Mater*. **2020**;*2*:204.
45. Johe KK, Hazel TG, Muller T, Dugich-Djordjevic MM, McKay RD. Single factors direct the differentiation of stem cells from the fetal and adult central nervous system. *Genes Dev*. **1996**;*10*:3129.
46. Liu Y, Dzidotor G, Le TT, Vinikoor T, Morgan K, Curry EJ, Das R, McClinton A, Eisenberg E, Apuzzo LN, Tran KTM, Prasad P, Flanagan TJ, Lee SW, Kan HM, Chorsi MT, Lo KWH, Laurencin CT, Nguyen TD. Exercise-induced piezoelectric stimulation for cartilage regeneration in rabbits. *Sci Transl Med*. **2022**;*14*:eabi7282.
47. Yuan T, Shao Y, Zhou X, Liu Q, Zhu Z, Zhou B, Dong Y, Stephanopoulos N, Gui S, Yan H, Liu D. Highly permeable DNA supramolecular hydrogel promotes neurogenesis and functional recovery after completely transected spinal cord injury. *Adv Mater (Deerfield Beach, Fla)*. **2021**. https://doi.org/10.1002/adma.202102428.
48. Basso DM, Beattie MS, Bresnahan JC. A sensitive and reliable locomotor rating scale for open field testing in rats. *J Neurotrauma*. **1995**;*12*:1.
49. Chaudhuri O, Cooper-White J, Janmey PA, Mooney DJ, Shenoy VB. Effects of extracellular matrix viscoelasticity on cellular behaviour. *Nature*. **2020**;*584*:535.
50. Reilly GC, Engler AJ. Intrinsic extracellular matrix properties regulate stem cell differentiation. *J Biomech*. **2010**;*43*:55.
51. Ozawa H, Matsumoto T, Ohashi T, Sato M, Kokubun S. Comparison of spinal cord gray matter and white matter softness: measurement by pipette aspiration method. *J Neurosurg*. **2001**;*95*:221.
52. Handorf AM, Zhou Y, Halanski MA, Li WJ. Tissue stiffness dictates development, homeostasis, and disease progression. *Organogenesis*. **2015**;*11*:1.
53. Hamid R, Averbeck MA, Chiang H, Garcia A, Al Mousa RT, Oh SJ, Patel A, Plata M, Del Popolo G. Epidemiology and pathophysiology of neurogenic bladder after spinal cord injury. *World J Urol*. **2018**;*36*:1517.
54. Li T, Shi C, Jin F, Yang F, Gu L, Wang T, Dong W, Feng ZQ. Cell activity modulation and its specific function maintenance by bioinspired electromechanical nanogenerator. *Sci Adv*. **2021**;*7*:eabh2350.
55. Xi K, Gu Y, Tang J, Chen H, Xu Y, Wu L, Cai F, Deng L, Yang H, Shi Q, Cui W, Chen L. Microenvironment-responsive immunoregulatory electrospun fibers for promoting nerve function recovery. *Nat Commun*. **2020**;*11*:4504.
56. Wang L, Zhu B, Deng Y, Li T, Tian Q, Yuan Z, Ma L, Cheng C, Guo Q, Qiu L. Biocatalytic and antioxidant nanostructures for ROS scavenging and biotherapeutics. *Adv Funct Mater*. **2021**. https://doi.org/10.1002/adfm.202101804.
57. Tang Q, Cao S, Ma T, Xiang X, Luo H, Borovskikh P, Rodriguez RD, Guo Q, Qiu L, Cheng C. Engineering biofunctional enzyme-mimics for catalytic therapeutics and diagnostics. *Adv Funct Mater*. **2020**. https://doi.org/10.1002/adfm.202007475.
58. Yang Z-y, Zhong Y-y, Zheng J, Liu Y, Li T, Hu E, Zhu X-f, Ding R-q, Wu Y, Zhang Y, Tang T, He F, Wang S-s, Wang Y. Fmoc-amino acid-based hydrogel vehicle for delivery of amygdalin to perform neuroprotection. *Smart Mater Med*. **2021**;*2*:56.
59. Cheng Z, Zhu W, Cao K, Wu F, Li J, Wang G, Li H, Lu M, Ren Y, He X. Anti-inflammatory mechanism of neural stem cell transplantation in spinal cord injury. *Int J Mol Sci*. **2016**. https://doi.org/10.3390/ijms17091380.
60. Tran AP, Warren PM, Silver J. The biology of regeneration failure and success after spinal cord injury. *Physiol Rev*. **2018**;*98*:881.
61. Volpato FZ, Fuhrmann T, Migliaresi C, Hutmacher DW, Dalton PD. Using extracellular matrix for regenerative medicine in the spinal cord. *Biomaterials*. **2013**;*34*:4945.
62. Zhang B, Su Y, Zhou J, Zheng Y, Zhu D. Toward a better regeneration through implant-mediated immunomodulation: harnessing the immune responses. *Adv Sci (Weinh)*. **2021**;*8*: e2100446.
63. Sun Y, Mu S, Xing Z, Guo J, Wu Z, Yu F, Bai M, Han X, Cheng C, Ye L. Catalase-mimetic artificial biocatalysts with Ru catalytic centers for ROS elimination and stem-cell protection. *Adv Mater*. **2022**;*34*: e2206208.
64. Tian Q, Wang W, Cao L, Tian X, Tian G, Chen M, Ma L, Liu X, Yuan Z, Cheng C, Guo Q. Multifaceted catalytic ROS-scavenging via electronic modulated metal oxides for regulating stem cell fate. *Adv Mater*. **2022**;*34*: e2207275.
65. Haggerty AE, Maldonado-Lasuncion I, Oudega M. Biomaterials for revascularization and immunomodulation after spinal cord injury. *Biomed Mater*. **2018**;*13*: 044105.
66. Hansen SM, Berezin V, Bock E. Signaling mechanisms of neurite outgrowth induced by the cell adhesion molecules NCAM and N-cadherin. *Cell Mol Life Sci*. **2008**;*65*:3809.
67. Mosher KI, Andres RH, Fukuhara T, Bieri G, Hasegawa-Moriyama M, He Y, Guzman R, Wyss-Coray T. Neural progenitor cells regulate microglia functions and activity. *Nat Neurosci*. **2012**;*15*:1485.
68. Ogata T. Therapeutic strategies for oligodendrocyte-mediated remyelination. *Adv Exp Med Biol*. **2019**;*1190*:265.
69. Schnadelbach O, Ozen I, Blaschuk OW, Meyer RL, Fawcett JW. N-cadherin is involved in axon-oligodendrocyte contact and myelination. *Mol Cell Neurosci*. **2001**;*17*:1084.
70. Hochmeister S, Romauch M, Bauer J, Seifert-Held T, Weissert R, Linington C, Hartung HP, Fazekas F, Storch MK. Re-expression of N-cadherin in remyelinating lesions of experimental inflammatory demyelination. *Exp Neurol*. **2012**;*237*:70.
71. Lai BQ, Zeng X, Han WT, Che MT, Ding Y, Li G, Zeng YS. Stem cell-derived neuronal relay strategies and functional electrical stimulation for treatment of spinal cord injury. *Biomaterials*. **2021**;*279*: 121211.
72. Fisher KM, Zaaimi B, Edgley SA, Baker SN. Extensive cortical convergence to primate reticulospinal pathways. *J Neurosci*. **2021**;*41*:1005.
73. Bai YR, Lai BQ, Han WT, Sun JH, Li G, Ding Y, Zeng X, Ma YH, Zeng YS. Decellularized optic nerve functional scaffold transplant facilitates directional axon regeneration and remyelination in the injured white matter of the rat spinal cord. *Neural Regen Res*. **2021**;*16*:2276.
74. Abematsu M, Tsujimura K, Yamano M, Saito M, Kohno K, Kohyama J, Namihira M, Komiya S, Nakashima K. Neurons derived from transplanted neural stem cells restore disrupted neuronal circuitry in a mouse model of spinal cord injury. *J Clin Invest*. **2010**;*120*:3255.
75. Malinverno M, Carta M, Epis R, Marcello E, Verpelli C, Cattabeni F, Sala C, Mulle C, Di Luca M, Gardoni F. Synaptic localization and activity of ADAM10 regulate excitatory synapses through N-cadherin cleavage. *J Neurosci*. **2010**;*30*:16343.

Kaiyuan Yang graduated from Tsinghua University and is now a resident at Department of Neurosurgery, Beijing Tsinghua Changgung Hospital, School of Clinical Medicine, Tsinghua University. His research focuses on the construction of multifunctional scaffolds for spinal cord repair.

Jia Yang graduated from Beijing University of Technology and is now a Ph.D. Student at the School of Materials Science and Engineering, Tsinghua University. Her research focuses on the construction of 3D bioprinting scaffolds for spinal cord repair.

Weitao Man graduated from Tsinghua University and is now a postdoctoral fellow at Massachusetts General Hospital, Harvard University. His research focuses on the construction of multifunctional scaffolds for spinal cord repair.

Zhe Meng graduated from Capital Medical University and is now a Ph.D. Student at the School of Clinical Medicine, Tsinghua University. His research focuses on the construction of multifunctional scaffolds for spinal cord repair.

Chun-Yi Yang is now a Ph.D. Student at the School of Materials Science and Engineering, Tsinghua University. His research interests focus on the use of functional polymer materials and their processing for spinal cord repair.

Zheng Cao graduated from Tsinghua University and is now a postdoctoral fellow at the School of Materials Science and Engineering, Tsinghua University. Her research focuses on the construction of multifunctional scaffolds for spinal cord repair.

Jun Liu is now a Ph.D. Student at the School of Materials Science and Engineering, Tsinghua University. His research focus on the drug delivery for biomedical applications.

Kunkoo Kim is now a postgraduate student at the School of Materials Science and Engineering, Tsinghua University. His research interests focus on the use of degradable biomaterials and their processing for biomedical applications.

Yaosai Liu graduated from Xuzhou Medical University and is now a Ph.D. Student at the School of Clinical Medicine, Tsinghua University. His research focuses on the construction of drug delivery scaffolds for spinal cord repair.

Shuhui Yang graduated from Tsinghua University and she joined the Zhejiang Sci-Tech University and the School of Materials Science and Engineering as an Associate Professor in 2022. Her research focuses on the construction of multifunctional scaffolds for peripheral nerve repair.

Yi Guo graduated from Capital Medical University and is now an Associate Professor at Department of Neurosurgery, Beijing Tsinghua Changgung Hospital, School of Clinical Medicine, Tsinghua University. His research focuses on the construction of degradable biomaterials for brain trauma repair.

Zhijun He is now a postgraduate student at the School of Clinical Medicine, Tsinghua University. He aims to develop nanoscale drug-delivery systems for use in spinal cord repair.

Chao Ma graduated from Capital Medical University and is now a Ph.D. Student at the School of Clinical Medicine, Tsinghua University. His research focuses on the construction of conductive biomaterials for spinal cord repair.

Guihuai Wang received his Ph.D. degree in neurosurgery from Capital Medical University in 1997. He is now working as a professor at Department of Neurosurgery, Beijing Tsinghua Changgung Hospital, School of Clinical Medicine, Tsinghua University. His research interests include the construction of nanomaterials and scaffolds for spinal cord repair and anti-tumor therapy.

Xiumei Wang received her Ph.D. degree in materials science and engineering from Tsinghua University in 2005. She worked as a postdoctoral fellow at University of Rochester and Massachusetts Institute of Technology from 2005 to 2008. She is now working as a professor at the School of Materials Science and Engineering, Tsinghua University. Her research interests include the fabrication of multifunctional biomaterials for tissue engineering and regenerative medicine.